Gallium-doped Zirconia Coatings Modulate Microbiological Outcomes in Dental Implant Surfaces

Authors

Agnese D'Agostino [a, b], Giulia Misiti [b], Alessandro Calogero Scalia [c], Matteo Pavarini [b], Andrea Fiorati [a, b], Andrea Cochis [c], Lia Rimondini [c], Vittoria Federica Borrini [d], Marcello Manfredi [d], Luca Andena [b], Luigi De Nardo [a, b] and Roberto Chiesa [a, b]

Affiliations

a. National Interuniversity Consortium of Materials Science and Technology (INSTM). Local Unit Politecnico di Milano, Milan, Italy

b. Department of Chemistry, Materials and Chemical Engineering "G. Natta" Politecnico di Milano, Milan, Italy

c. Department of Health Sciences, Center for Translational Research on Autoimmune & Allergic Diseases CAAD, Università del Piemonte Orientale UPO, Novara, Italy

d. Department of Translational Medicine, Center for Translational Research on Autoimmune and Allergic Disease – CAAD, Università Del Piemonte Orientale UPO, Novara, Italy

Corresponding Author

Agnese D'Agostino

agnese.dagostino@polimi.it

Department of Chemistry, Materials and Chemical Engineering "G. Natta"

Politecnico di Milano

Via Mancinelli, 7

20131 Milan

Italy

Abstract

Peri-implantitis remains a severe complication, despite the significant advances in manufacturing materials supporting advanced therapies. Herein a sol-gel process is performed to easily gain antibacterial zirconia coatings onto bulk zirconia, which is becoming very popular for realizing abutment in dental implantology. The coatings' physicochemical properties were analyzed through XRD and SEM-EDS investigations. Scratch resistance and static contact angle measurements studied their stability and wettability. Uniform tetragonal zirconia coatings doped with gallium were obtained with optimal mechanical stability and hydrophilic behavior. The biological investigations pointed out that gallium-doped zirconia coatings: (i) displayed fully cytocompatibility towards human gingival fibroblasts (HGF); (ii) exhibited significant antimicrobial activity against the *A. actinomycetemcomitans* pathogen; (iii) were able to preserve the commensal *S. salivarius*. Furthermore, the proteomic analyses revealed that the presence of Ga didn't impair the normal oral microbiota. Still, interestingly, it decreased by 17% the presence of *Fusobacterium nucleatum*, a Gram-negative, strictly anaerobic bacteria that naturally present in the gastrointestinal tract. So, the herein approach could be a valid starting point to develop coatings to easily improve zirconia dental implant performance.

Keywords: zirconia; sol-gel coatings; gallium; antibacterial activity; proteomic analyses; oral microbiota

1. Introduction

Materials intended for dental application should help soft tissue regeneration reducing at the same time bacterial contamination. The latter, when overabundant, may cause first peri-implant mucositis and then peri-implantitis, a pathological condition that, if not treated, will lead to bone loss [1,2]. Metallic implants, particularly titanium and its alloys, have always been considered the gold standard in many medical and dentistry applications thanks to their optimal biocompatibility and outstanding mechanical characteristics. However, using the titanium family as material for the abutments has been debated over the years due to the unsightly grey color it creates around the soft tissues [3]. To overcome this problem, alumina and zirconia have been considered optimal candidates. The first has good biological and esthetic properties, creating a peri-implant mucosa similar to the one generated by titanium implants but possessing a lower fracture strength than the titanium and zirconia [4]. On the other hand, the use of zirconia in dentistry holds several advantages: i) it possesses excellent chemical stability with relatively high mechanical properties, and can promote “contact osteogenesis” [5]; ii) it improves aesthetics in the area surrounding the gingival soft tissues, crucial in dental procedures; iii) it naturally reduces the extreme bacterial contamination.

As far as antimicrobial properties are concerned, *in vitro* results are slightly in contrast and are highly dependent on the bacterial species considered. It has been pointed out that zirconia is generally superior to titanium in inhibiting bacterial adhesion [6] while it has also been demonstrated that *S. mutans* better colonize polished zirconia in comparison to titanium [7]. *In vivo* studies display more homogeneous results: a decrease in bacterial adhesion and colonization on zirconia compared to titanium implants has been proved [8,9]. However, considering that materials intended for dental application must face unavoidable contact with the hundreds of bacterial species (both pathogenic and commensal) belonging to the oral microbiome [10], it is crucial to functionalize the material to reduce as much as possible the presence of pathogenic bacteria that may have a role in different medical conditions maintaining the commensal species.

Among all the treatments, the use of inorganic ions (Ag^{+}, Cu^{2+}, and Zn^{2+}) as a coating for many materials is still the most effective [11–14]. Unfortunately, considering their ability to target cell membranes, ribosomes, and genetic material, their effect is unpredictable, and the action is not targeted [15–17]. This broad-spectrum activity may lead to oral dysbiosis, creating favorable conditions for the growth of pathogenic bacteria. A solution can be represented by gallium (Ga^{3+}) which is gaining attention thanks to its ability to mimic Iron

ions (Fe^{3+}) and interfere with bacterial metabolism. In fact, Ga^{3+} is similar to Fe^{3+} in terms of charge, ionic radius, coordination number and electronic configuration. Nevertheless, Ga^{3+} cannot be reduced to a lower oxidation state, as of Fe^{3+}, and this may block siderophores, hindering several bacteria biological functions. [18]

Surface modification of implants by coatings could represent an optimal compromise for improving required features such as biocompatibility and osseo-integration and providing additional properties like antibacterial activity to avoid implant failure [19–23]. Nowadays, the development of functional coatings by the sol-gel technology is foremost pursued since this method enables a very high versatility in composition, shape control, low-cost processing, and significant tuning over the final microstructure [24]. Typically, the sol-gel process is based on four main steps: (i) synthesis of the 'sol' from hydrolysis and partial condensation of metal alkoxides or metal chlorides; (ii) formation of the gel via poly-condensation to develop metal–oxo–metal or metal–hydroxy–metal bonds; (iii) 'aging' where condensation carries on within the gel network; (iv) drying the gel to form a dense 'xerogel' or an aerogel (through supercritical drying). Since several parameters affect the sol-gel process, such as the type of precursor, the pH, the catalysts, the precursor, the water ratio, the solvents, and the temperature [24,25], the final properties of obtained material can be tuned to fit specific needs.

Sol-gel coatings of titanium dioxide (TiO_2), silica (SiO_2), zirconia (ZrO_2), as well as hydroxyapatite (HA), have been employed to coat titanium, Cobalt-Chromium-Molybdenum (Co-Cr-Mo), and zirconia implants to enhance their biocompatibility, in terms of cytocompatibility and osseointegration [23,26,27], exerting bactericidal effect [23,28], and providing corrosion protection [25,29–31]. Recently, the use of the sol-gel technique combined with spin-coating deposition and followed by the proper thermal treatment allowed the tailoring of thin ZrO_2 films with a determined and reproducible crystalline phase and thickness as well as a controlled microstructure [32,33]. Furthermore, it has been proven that doped ZrO_2 coatings with calcium ions (Ca^{2+}) [32] or gallium ions (Ga^{3+}) [33] promote the proliferation of Saos-2 human osteoblastic cells and exert antibacterial activity against oral pathogens *Porphyromonas gingivalis* and *Aggregatibacter actinomycetemcomitans* [33]. Even if zirconia is becoming very popular in implant dentistry because of the aesthetic reasons as well as a growing demand for metal-free components [34,35], there are only few studies concerning surface modifications of this material by sol-gel approach to mitigate bacterial colonization and to avoid the risk of peri-implantitis [36,37].

The current study exploited the sol-gel spin coating process to realize zirconia coatings onto bulk zirconia used to manufacture abutments. To confer antibacterial activity, gallium was chosen as a doping agent. XRD analyses confirmed the stabilization of the tetragonal zirconia phase; SEM-EDS investigation revealed that coatings, although they showed some micro-cracks, uniformly covered substrates and corroborated the inclusion of gallium within layers; the mechanical evaluation, in terms of scratch resistance, showed no delamination of coatings; static contact angle measurements attested the hydrophilic behavior of zirconia coatings. Furthermore, specimens' cytocompatibility was affirmed towards gingival fibroblasts, and gallium-doped zirconia coatings were able to significantly reduce the viability of the pathogen *Aggregatibacter actinomycetemcomitans* as well as to preserve the commensal *Streptococcus salivarius.* Finally, the effect of doped coatings on human oral plaque supported that gallium does not affect the normal oral microenvironment and, at the same time, could decrease the presence of *Fusobacterium nucleatum*, a Gram-negative, strictly anaerobic bacteria naturally present in the gastrointestinal tract.

2. Materials and Methods

2.1 Materials

All chemicals were purchased by Merck (Italy) and used without any purification: Zirconium (IV) chloride ($ZrCl_4$); Ethanol (EtOH); Pluronic F-127 (poly(ethylene oxide)$_{106}$-poly(propylene oxide)$_{70}$-poly(ethylene oxide)$_{106}$, PEO_{106}-PPO_{70}-PEO_{106}) block copolymer; Gallium (III) nitrate hydrate ($Ga(NO_3)_3{\cdot}H_2O$). Millipore water was employed for the preparation of aqueous solutions. Polycrystalline zirconia discs, 1 mm thick and 15 mm in diameter (supplied by Zirkonzahn GmbH, Gais, Italy) were used as substrates for the coatings. Disc surfaces were sterilized with ethanol (EtOH) before functionalization.

2.2 Sol-gel synthesis and coatings preparation

Zirconia coatings were synthesized by sol-gel spin coating method as described previously [33]. Briefly, two solutions were prepared in 2 mL of an ethanol/water solution (9:1) by dissolving 0.35 g of $ZrCl_4$ and 1.7 g of Pluronic F-127, respectively. Zirconia solution was obtained by adding the first solution to the second one. Similarly, gallium-doped zirconia solution was prepared by solubilizing 20% mol/mol of $Ga(NO_3)_3{\cdot}H_2O$ to the starting $ZrCl_4$ solution. Coatings were prepared after depositing 0.3 mL of zirconia solution or Ga-doped zirconia solution by micropipette on bulk zirconia disc and using the spin coater (Laurell

Model WS-650SZ-8NPP/LITE) with a ramp of 10 s to 200 rpm, followed by 30 s at 300 rpm. The functionalized zirconia discs were kept in closed vessel and consolidated for 2 h at 100 °C. Calcination treatment was performed in the programmable muffle furnace (Carbolite Gero RHF-1400) at 400 °C in air for 3 h. Samples were tagged Z or ZGa, where Z was used to identify the no doped zirconia samples, while ZGa was utilized for Ga-doped zirconia coatings.

2.3 Physicochemical characterization

X-ray analysis was conducted to study the crystalline phase induced by the calcination treatment at 400 °C. The XRD Philips PW1830 diffractometer operating with Bragg-Brentano camera geometry and Cu Kα incident radiation (wavelength λ = 0.154056 nm) was used. X-ray diffraction patterns were collected at room temperature (2θ within 10–70) setting 0.5 s as scanning time per step. Identification of crystalline phase was carried out by using Panalytical XPert Data software equipped with JPCDS database.

The morphology as well as the elemental composition of the coatings was carried out by a scanning electron microscope (EVO 50 SEM, Zeiss, Germany) at 15 kV operating in secondary electron mode (SE) and back scattering mode (BSE) equipped with energy dispersive X-ray detector (QUANTAX EDS, Bruker, Germany).

The adhesion and stability of the sol-gel coatings was assessed by scratch testing using a Micro-Scratch Tester (MST, CSM Instruments, CH) on both coated and uncoated zirconia samples. The scratches were performed with a 200 µm, 120° Rockwell C spherical-conical diamond tip, in accordance with the ASTM C1624-22 standard [38]. Five 5 mm long scratches were performed per specimen by applying a progressive loading test mode, with load increasing from 0.03 N to 30 N at a rate of 60 N/min (10 mm/min), and data about transversal force, acoustic emission, profile depth and residual depth were recorded with an acquisition rate of 20 Hz. The samples were then observed by SEM to evaluate the appearance of the scratches. In this work, both the SEM micrographs and the recorded acoustic emission (AE) during scratch were considered as the main methods for identifying the critical loads of the coatings.

Wettability properties of coatings were evaluated through static contact angle. The sessile drop method was chosen to determine the contact angles values. Drops of distilled water (0.05 mL) were deposited on each sample and examined with goniometer instrumental set-up equipped with a software for image elaboration (Drop Shape Analysis). Five measurements were taken for each sample, replicated twice.

2.4 *In vitro* cytocompatibility evaluation

Prior to biological assays, zirconia coated discs (Z and ZGa samples) have been sterilized under UV light for 30 minutes each side.

2.4.1 Cells cultivation

Specimens cytocompatibility assessment was verified by using primary human gingival fibroblasts (HGF) purchased from American Type Culture Collection (ATCC PCS-201-018). Cells were cultivated in alpha-modified Minimal Essential Medium (α-MEM, from Sigma), 10% fetal bovine serum (FBS, Lonza), and 1% antibiotics. Cells were maintained at 37 °C, 5% CO_2 atmosphere, and 95% humidity. When confluency reached 80-85% cells have been detached with trypsin-EDTA solution (0,25%), harvested, and used for the *in vitro* experiments.

2.4.2 Cytocompatibility assessment

Following the manufacturer's instruction, cell viability was determined through metabolic activity using the Alamar blue assay (alamarBlue, Thermo-Scientific). Sterile specimens (Z and ZGa) were individually placed into a sterile 12-multiwell plate; A defined number of HGFs (2×10^4 cells/specimen) were dropwise spotted directly onto the specimens' surface and maintained in the incubator for 3-4 hours, allowing cells' adhesion and spread. Afterward, each well was rinsed with 1 ml of complete medium, and cells were cultivated for 72 h at 37 °C, 5% CO_2.

The Alamar blue solution (0.015% in PBS) was added to the wells, and the plate was maintained for 4h in the dark at 37 °C. Later, 100 µl were collected from each specimen and transferred to a dark 96 wells plate; fluorescence signals were evaluated by a spectrophotometer (Spark, Tecan Trading AG, Mannedorf, Switzerland) using a fluorescence excitation wavelength of 530 nm and a fluorescence emission reading of 590 nm. Moreover, the adhesion, spread, and morphology of cells cultivated onto the specimens' surface were visually checked by using immunofluorescence (IF) and scanning electron microscopy (SEM). Immunofluorescence was performed as follows: cells were fixed in 4% paraformaldehyde in PBS for 1h at RT and then washed twice with PBS. Following 5 minutes of permeabilization of cells in Triton 0,2% in ice, samples were incubated with 1:500 Phalloidin-TRITC and 1:1000 DAPI diluted in PBS/0,1% BSA for 45 minutes, washed twice with PBS and observed under a fluorescent microscope (EvosFloid, ThermoFisher, Waltham, Massachusetts, USA). Specimens' preparation for scanning electron microscopy was performed as follows: cells were fixed in 2,5%

glutaraldehyde for 1h at RT and then washed with PBS. Specimens' dehydration was achieved by increasing the ethanolic scale from 50 to 100% for 1h each. Thereafter, specimens were submerged in hexamethyldisilazane (HMDS) for 20'. Scaffolds were sputtered with a gold layer (10nm layer by SmartCoater, Jeol, Akishima, Tokyo, Japan) and then visualized under the scanning electron microscope (JSM-IT500 InTouchScope™ Scanning Electron Microscope, Jeol, Akishima, Tokyo, Japan).

2.5 Antibacterial activity evaluation

2.5.1 Bacteria growth conditions

To assess materials' antibacterial activity, *Aggregatibacter actinomycetemcomitans* (ATCC 33384), a Gram-negative bacterium commonly responsible for oral infections leading to periodontal and peri-implant diseases, and *Streptococcus salivarius* (DSM 20067), a Gram-positive bacterium considered as commensal, were considered. The bacteria were cultivated in trypticase soy agar plates (TSA, Sigma-Aldrich) and incubated at 37 °C until single round colonies were formed; then, a few colonies were collected and spotted into 15 ml of Tryptic soy broth (TSB, Sigma-Aldrich) and incubated overnight at 37 °C under agitation (120 rpm). The day after, a fresh broth culture was prepared before the experiment by diluting bacteria into a fresh medium until a final concentration of 1×10^5 bacteria/ml corresponding to a spectrophotometric optical density of 0.001 read at 600 nm wavelength.

2.5.2 *In vitro* antibacterial test

The metabolic activity of bacteria in contact with functionalized materials were evaluated using the colorimetric-metabolic assay Alamar blue, performed as previously described (0,0015% in PBS). Sterile specimens were individually placed into a sterile 12-multiwell plate. 300 µl of the bacterial suspensions containing 1×10^5 bacteria/specimen, prepared as previously described, was put in contact with the material's surface.

2.5.3 Preparation of oral plaque

To determine the selective ability of gallium in killing pathogenic bacteria and preserving the commensal ones in a more realistic scenario, specimens were put in contact with oral plaque. Samples of oral plaque were collected from 3 healthy volunteers by non-invasive procedures and after obtaining their informed consensus under the Declaration of Helsinki. Oral plaque samples were taken from supragingival parts of premolars or molars with

individual sterile Gracey curettes by gently scraping. After their removal, samples were pooled and maintained in sterile cooked meat culture broth (Merck, Darmstadt, Germany). Microorganisms were dispersed by vortex, transferred in 30 ml of fresh media, and maintained under anaerobic conditions (Baker Ruskinn Concept 400 Workstations), allowing most of the oral species to grow. After 24 h, the bacterial community of oral plaque was frozen and stored at −80 °C to preserve the starting population.

2.5.4 Population assessment

To assess the gallium effect on oral plaque, extracted and expanded as previously described, samples were submerged into 500 µl of bacterial suspension containing 1×10^5 bacterial cells, adjusted accordingly with the optical density at 600 nm. After incubation in anaerobic conditions for 24 h, bacterial biofilm derived from both samples (with and without gallium) were washed once with PBS solution to remove unattached bacterial cells and sonicated three times (5 min followed by 30 s vortex). The solution containing biofilm bacteria detached as previously described were transferred into a new sterile test tube and centrifuged at 10,000 rpm for 10'. Moreover, bacteria-contaminated material surfaces and biofilm features and development were SEM checked as previously described.

2.5.5 Protein extraction and digestion

Protein extraction was performed on biofilm formant bacteria by adding 200 µl of lysis buffer, composed of 8 M urea buffer (pH 8.5) and Tris-HCl, to all samples obtained in the previous section. To allow the complete bacterial cells' proteins release, the samples were sonicated 6 times (27% amplitude for 10s followed by 10s in ice). After protein quantification was assayed by using Bradford reagent (Sigma-Aldrich), a volume of protein samples equals to 80 µg (selected threshold concentration) was added to 25 µl of 100 mM ammonium bicarbonate (NH_4HCO_3). For protein reduction, 15 µl trifluoroethanol (TFE, 99%) and 2.5 µl of dithiothreitol (200 mM DTT stock solution) (Sigma-Aldrich) solutions were added and kept at 60 °C for 30 min. Furthermore, proteins were alkylated with 10 µL of cysteine blocking reagent (Iodoacetamide, IAM, 200 mM; Sigma-Aldrich) for 30 min at room temperature in the dark digested with trypsin (Promega, Sequence Grade) overnight at 37 °C. Trypsin activity was stopped by adding 2 µL of neat formic acid, and the digests were dried by speed vacuum.

2.6 Proteomics analysis

To investigate the impact of gallium on the oral biofilm collected from healthy volunteers, proteomics analysis was performed following a well-established methodology [39] on the protein samples prepared in the previous section. Briefly, the digested peptides were analyzed with an Ultra-High-Performance Liquid Chromatography (UHPLC Vanquish system, Thermo Scientific, Rodano, Italy) coupled with an Orbitrap Q-Exactive Plus (Thermo Scientific, Rodano, Italy). Peptides were separated by a reverse phase column (Accucore™ RP-MS 100 x 2.1 mm, particle size 2.6 µm), maintained at a constant temperature of 40 °C at a flow rate of 0.2 mL/min. The mass spectra analysis was carried out using Mascot v.2.4 (Matrix Science Inc., Boston, USA): trypsin was selected as digestion enzyme with 2 missed cleavages. A search tolerance of 10 ppm was specified for the peptide mass tolerance, and 0.1 Da for the MS/MS tolerance. The charges of the peptides to search for were set to 2þ, 3þ, and 4þ, and the search was set on monoisotopic mass. The following modifications were specified for the search: carbamidomethyl cysteines as fixed modification and oxidized methionine as variable modification. The Human Oral Microbiome Database V3 was used, and a target-decoy database search was performed. The false discovery rate was fixed at 1% [40]. Peptides were mapped to their respective taxa of origin using Unipept [41].

2.7 Statistical analysis of data

Statistical analysis was carried out by GraphPad version 6 (GraphPad Software, CA, USA). *In vitro* cytocompatibility and antibacterial activity evaluation was performed in triplicate, while the test of contact with the oral plaque was assessed using 6 samples. Groups were compared by the one-way ANOVA using Tukey's test as a post-hoc analysis. Significant differences were established at $p < 0.05$.

3. Results and Discussion

3.1 Physicochemical and morphological characterizations of zirconia coatings

It is well known that zirconia exists in three different crystal structures based on the calcination temperatures: monoclinic up to 1100 °C, tetragonal at 1100–2370 °C, and cubic above 2370 °C [42]. The martensitic transformation (the tetragonal to monoclinic transformation) leads to a volume change, resulting in internal stresses in the zirconia structure, thereby cause cracking of the bulk, and delamination, and peeling of the coating. Since the tetragonal zirconia exhibits high strength and toughness, stabilizing this phase is

crucial for biomedical applications [43]. The investigation of the crystalline structure of both zirconia discs and sol-gel zirconia coatings was conducted through XRD analysis. **Fig. 1** reports the XRD patterns of uncoated zirconia disc (bulk), thermally treated at 400 °C ($bulk_{400}$), as well as sol-gel zirconia powders calcined at 400 °C (Z). Bulk and $bulk_{400}$ were found to consist of baddeleyite (monoclinic zirconia) with the characteristic peaks at 2θ = 28.2°, 31.5°, 34.2 ° (PDS 98-006-0900) and nanocrystalline zirconium oxide (tetragonal zirconia) with sharp peaks at 2θ =30.22°, 35.21°; 50.32°; 60.02° (PDS 98-015-7619). The tetragonal zirconia phase is even predominant in Z specimen (PDS 00-007-0337), indicating that this sol-gel spin-coating approach enables the realization of tetragonal zirconia coatings onto the zirconia disc surface.

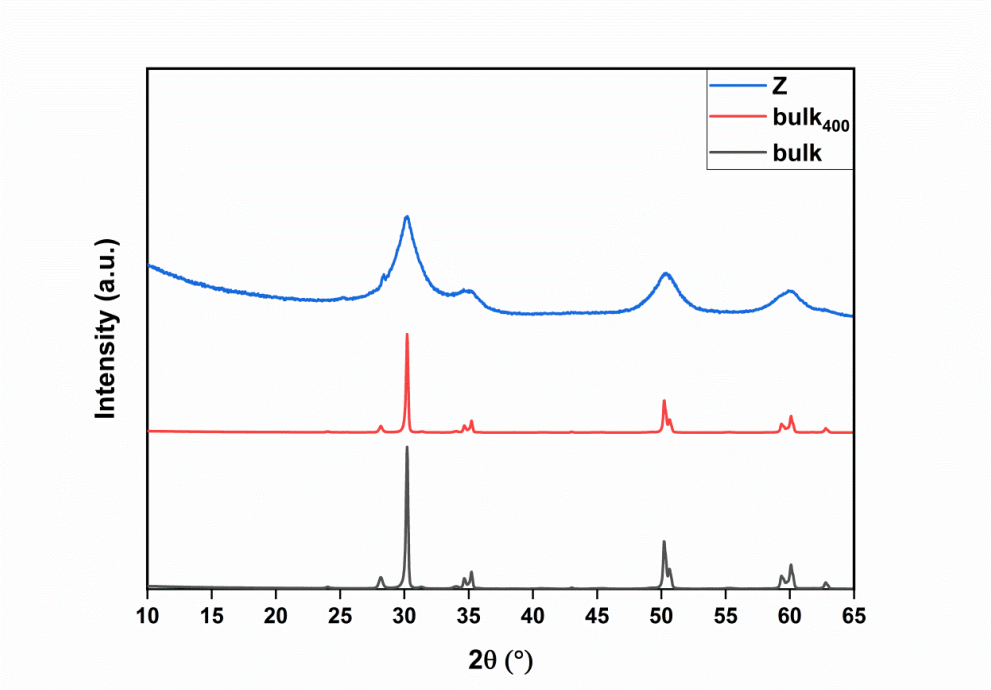

Fig. 1. XRD patterns of bulk (grey line), $bulk_{400}$ (red line) and Z (blue line).

Fig. 2 reports the coated zirconia disc (Z) micro-morphological characterization *via* SEM. Secondary (SE) and backscattered electrons (BSE) micrographs show a uniform sol-gel coating morphology on Z specimens. (**Fig. S1** compares the coating to the uncoated zirconia disc.) Nevertheless, the coating is not continuous, and some micro-cracks can be detected on the surface. The main reasons for the crack formation are ascribed to the fast ethanol evaporation during the drying process and the thermal expansion between the coatings and substrate [23,44]. Since the substrate and the coating mainly consisted of zirconia, there are no differences in the respective EDS spectra (**Fig. S2**). Consequently,

the mapping of the zirconium (Zr), as well as the oxygen (O), indicated that these elements co-exist and are uniformly distributed (**Fig. 2C**).

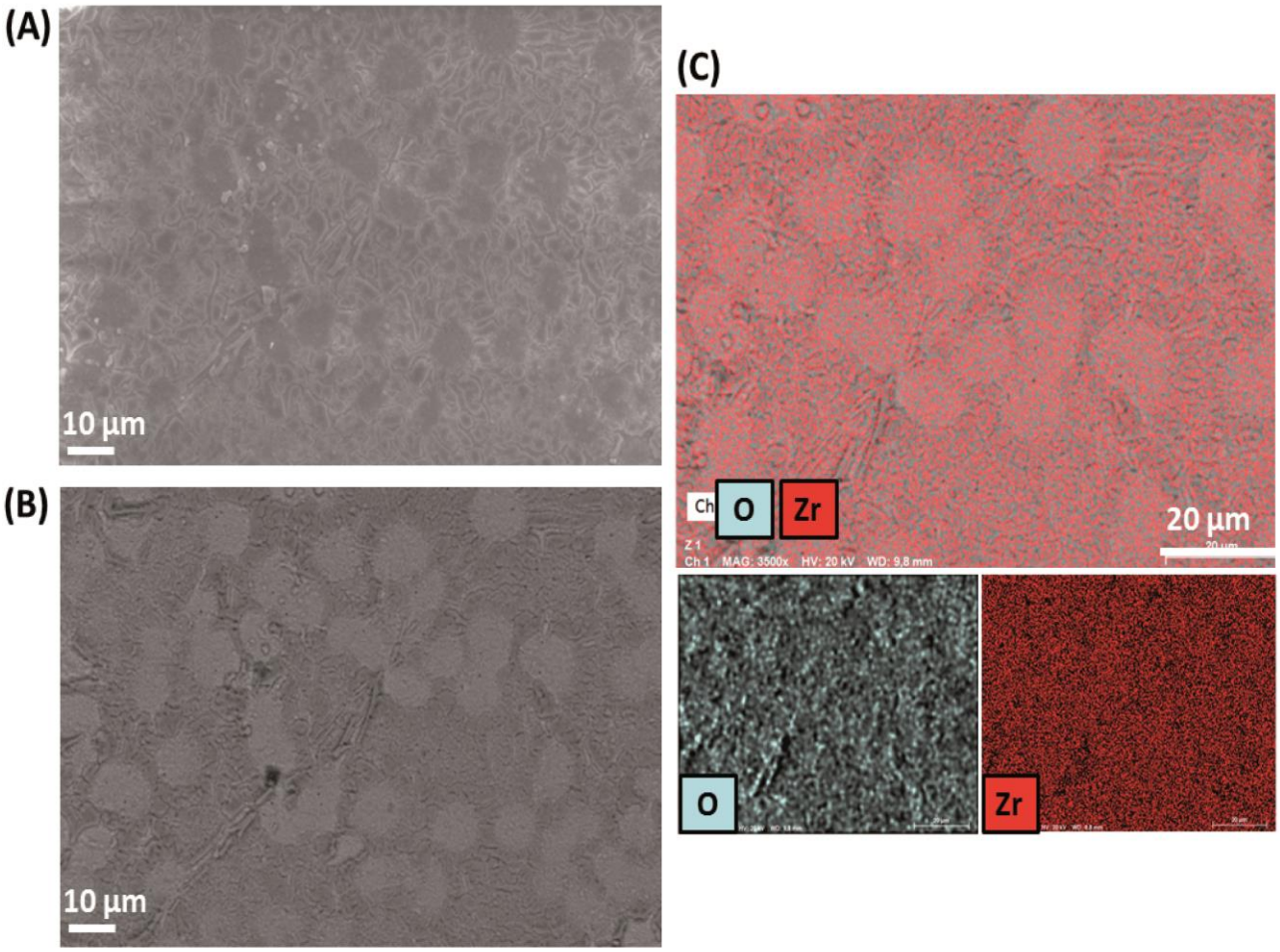

Fig. 2. SEM-EDS observation of Z sample at 3.5 Kx: **(A)** SE micrograph, **(B)** BSE micrograph, **(C)** EDS elements mapping of oxygen and zirconium.

Fig. 3 displays the morphology and the microanalysis of the Ga-doped zirconia coatings (ZGa sample). SE and BSE micrographs reveal that the coating is cracked. Indeed, the BSE image (**Fig. 3B**) highlights a variation of gray levels of coating with respect to non-coated areas of the zirconia disc. Since this compositional contrast corresponds to a variation in chemical composition, the coating will contain an element with a lower atomic number that generates fewer backscattering electrons, and the EDS spectrum confirmed it was gallium (**Fig. S3)**. Moreover, elements mapping confirmed that the doping agent is included in the zirconia coating (**Fig. 5C**).

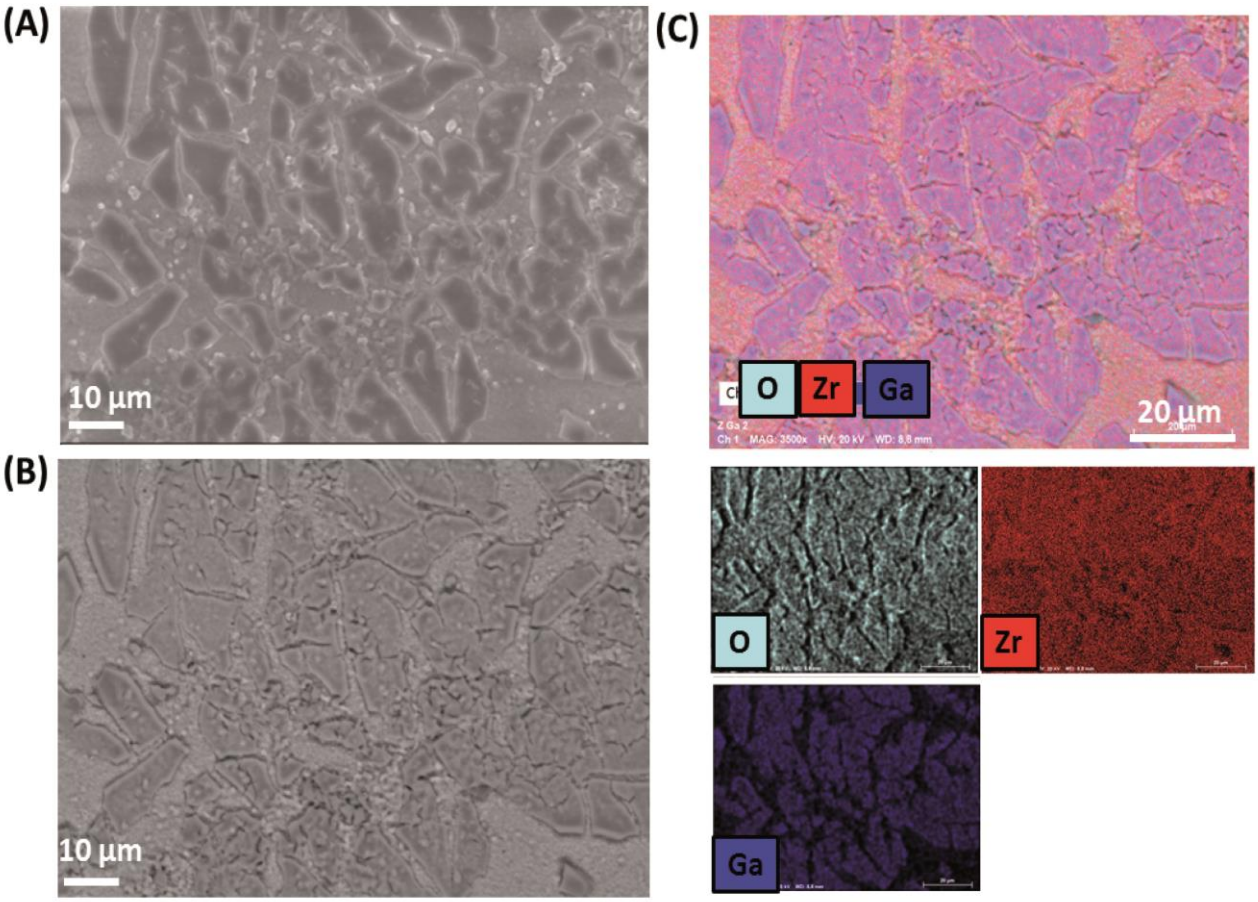

Fig. 3. SEM-EDS observation for ZGa sample at 3.5 Kx: **(A)** SE micrograph, **(B)** BSE micrograph, **(C)** EDS elements mapping of oxygen, zirconium, and gallium

3.2 Mechanical stability and wettability properties

The mechanical properties of the coating were assessed in terms of scratch resistance by comparing the behavior of the coating to that of an uncoated zirconia disc (bulk). From the SEM micrographs, it was possible to observe the initial scratching after load application (L_{c1}, **Fig. 4B**) from 0.2 ÷ 0.3 N. For the uncoated samples, the acoustic emission highlighted only a few sharp peaks (**Fig. 4C**) due to the indenter sliding on the smooth ceramic surface. The same behavior was observable on the coated samples, but only at F < 10 N, after which the coating's cohesive strength was overcome and cracking started (L_{c2}). The complete coating detachment from the substrate (L_{c3}, **Fig. 4D**) was observed for loads higher than 19 N, representing an estimation of the adhesive strength of the coatings.

The observed critical load values were consistent or slightly higher than the literature data [45]. Overall, no delamination was present, and the surface was continuous in the areas surrounding the scratch, indicating optimal coating stability.

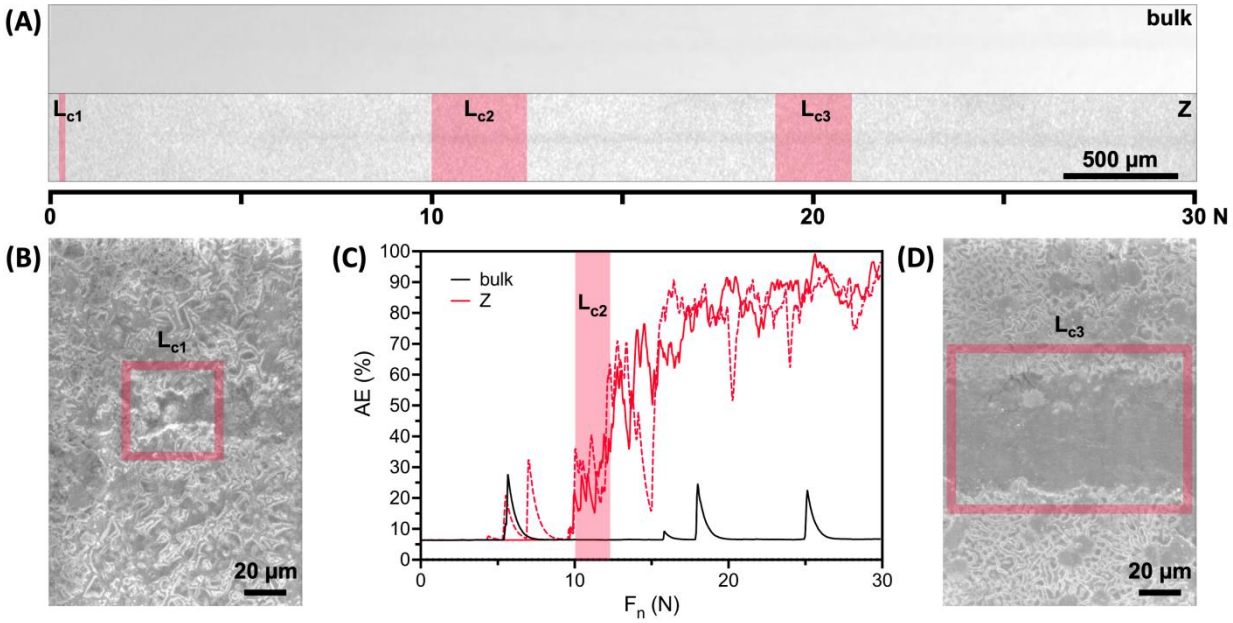

Fig. 4. (A) Low magnification SEM micrographs of representative scratches on uncoated (bulk) and coated (Z) zirconia samples, highlighting the regions corresponding to the observed critical loads (L_c). The bars indicate both the image scale and the corresponding load applied. **(B)** High magnification SEM image of a scratch on coated zirconia in the L_{c1} region (initial scratching). **(C)** Acoustic emission (AE) vs. applied normal load plot for both uncoated and coated samples, highlighting the L_{c2} region (coating cracking). **(D)** High magnification SEM image of a scratch on coated zirconia in the L_{c3} region (full coating detachment).

The surface wettability of a dental implant material is an important parameter that influences protein adsorption dynamics and, thus, cell adhesion and proliferation: it further affects bacterial adhesion and subsequent biofilm formation [46]. Typically, the cells' (i.e., fibroblast, osteoblast) adhesion, proliferation, and differentiation may be facilitated on hydrophilic surfaces, with a contact angle lower than 90°, compared to hydrophobic ones, characterized by a contact angle higher than 90°. Even if the debate concerning the possible mechanisms of bacterial adhesion is still open owing to the multifactorial nature of peri-implantitis, it has been pointed out that bacteria with hydrophilic properties prefer to attach to hydrophilic surfaces and vice versa [46,47]. In **Fig. 5,** the contact angle measurements for bulk, Z, and ZGa samples are summarized: Z and ZGa specimens exhibited a more hydrophilic behavior respect to bulk sample. In addition, the inclusion of

gallium within zirconia coatings enabled the decrease of contact angle values, as previously demonstrated [33].

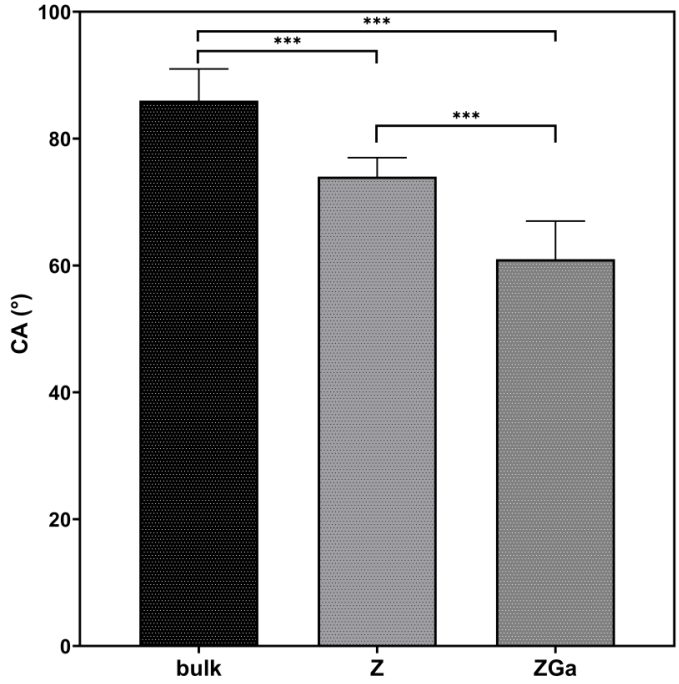

Fig. 5. Contact angle measurements of bulk, Z and ZGa samples. All values are expressed in terms of average ± standard deviation. (*p < 0.05, **p < 0.005, ***p < 0.0005).

3.3 Biological investigation

Specimens' cytocompatibility results are represented in **Fig. 6**. The metabolic activity of cells cultivated onto the disc containing gallium remains comparable to the one of the bare material for all the time points in exam (24 h, 48 h, 72 h; p>0.05), thus demonstrating that safety is not related to time of gallium exposure. Moreover, as confirmed by the immunofluorescence and the scanning electron microscope, cell morphology and spread are well-preserved. As already mentioned in the introduction, gallium can be considered as a good alternative for other inorganic ions like silver [14] and copper [11], very effective in preventing bacterial attachment and proliferation but potentially deleterious also for eukaryotic cells. Indeed, gallium (Ga^{3+}) mimicking Iron (Fe^{3+}), efficiently block bacterial metabolism being at the same time safe for cells, as already demonstrated [18,23,33,48].

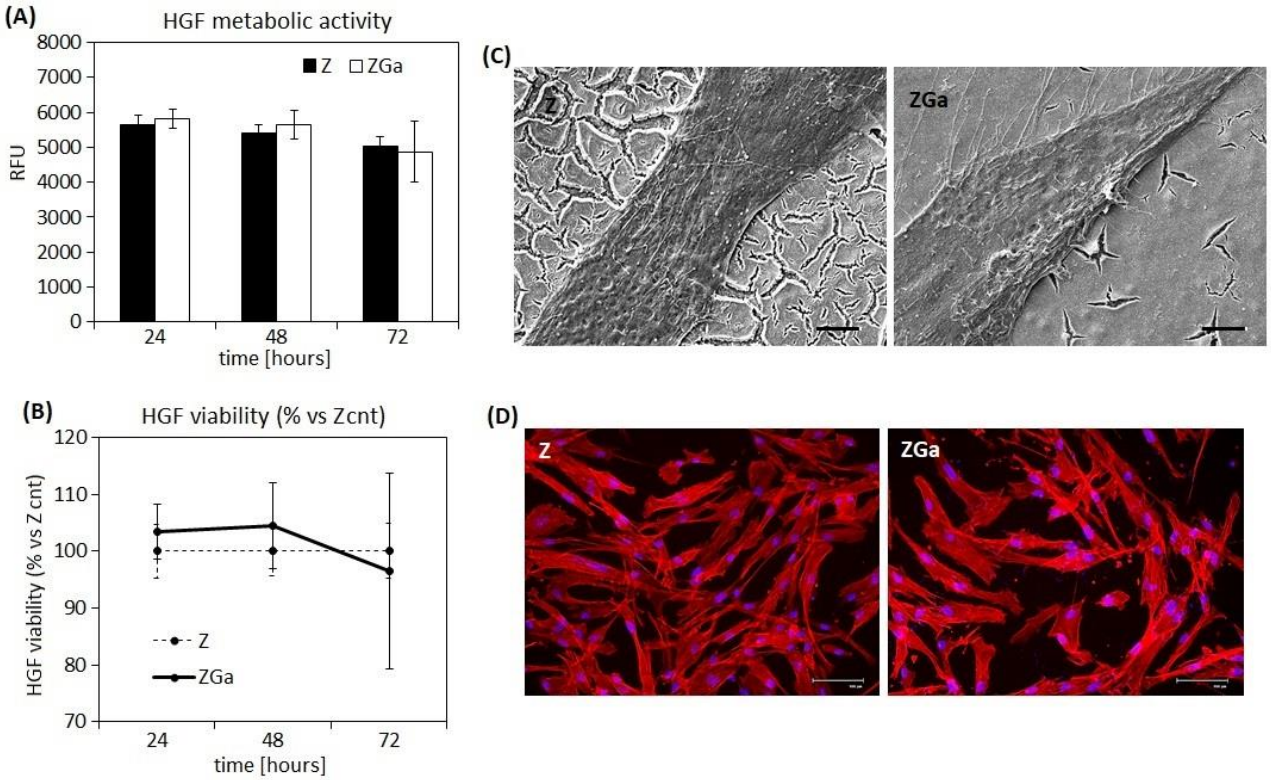

Fig. 6. Specimens' cytocompatibility results. Metabolic activity and viability of cells cultivated on no doped zirconia samples (Z) and Ga-doped zirconia samples (ZGa) are represented in **(A)** and **(B)** respectively. No significant differences have been noticed ($p > 0.05$). Cells' morphology, spread and distribution on both scaffolds are represented by **(C)** Scanning Electron Microscopy (scale bar 5 µm) and **(D)** immunofluorescence (scale bar 100 µm).

To assess the antimicrobial effect of the gallium-doped material, two bacterial strains, one pathogen and one commensal, and a pool of oral plaque derived from healthy volunteers were used. This pathogen/commensal comparison may help to confirm gallium selectivity against the former. Results are reported in **Fig. 7B-C**. The coating effect on the single bacterial strains is diametrically opposite: Indeed, in *A. actinomycetemcomitans* we can notice a similarity between the samples during the first 24h followed by a significative reduction in the metabolic activity during the 2nd time point. On the contrary, this trend is not present in the commensal bacteria for which the metabolic activity remains unaltered for both materials in both time points. These results match with the previous work in which the gallium coating was able to reduce significantly the viability of the pathogen preserving the commensal [33]. As already observed elsewhere, the selective effect of the gallium may be related to the higher capability of pathogens in uptake quickly nutrients from the environment in comparison to the commensal strains [33,49].

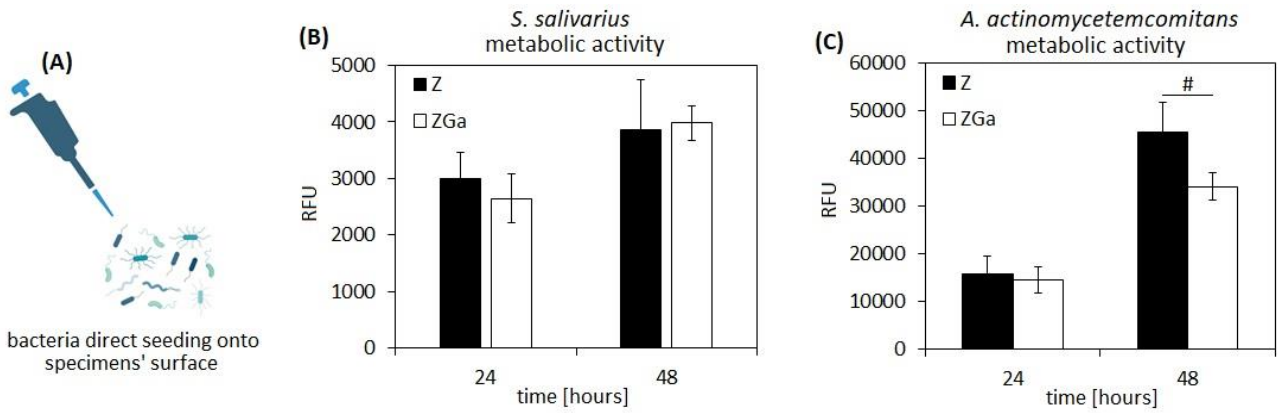

Fig. 7. Single strains antibacterial effect. **(A)** Cartoon representing the infection methodology. The metabolic activity of the commensal and pathogenic bacteria is represented in **(B)** and **(C)** respectively. In the commensal there are no significant differences ($p > 0.05$) between the materials after 24 and 48 h from the contact. In the pathogen, after 24 h from the contact we can't notice a significant difference between the no doped and the doped scaffold ($p > 0.05$) but after 48 h the gallium-doped specimens reduce significantly ($p < 0.05$) the AA metabolic activity.

Once the selective effect of gallium had been confirmed on single strains, to assess the Ga-coated material's effect on the normal human microbiota the coated materials were tested in contact with the oral plaque collected from 3 healthy volunteers (**Fig. 8)**. The analysis of proteins extracted from the oral plaque of the healthy volunteers in contact with the no-doped zirconia coatings or the Ga-doped materials led to the identification of 40 bacterial species. Only 11 species representative of more than 1% of the population were considered for the comparison. (The remaining 29 are listed in **Table S1**.)

The presence of gallium did not impair the normal oral microenvironment. Still, at the same time, it was able to decrease by 17% the presence of *Fusobacterium nucleatum*, a Gram-negative strictly anaerobic bacteria naturally present in the gastrointestinal tract (GI), from the oral cavity to the colon [50]. All GI sites have stable microbiota, essential for several physiological processes. The oral microbiota (OM) comprehends over 700 bacterial species, of which 200 are stably colonized. Oral dysbiosis, mainly caused by chronic alcohol intake and poor dental hygiene, increases the number of pathogenic bacteria like the *F. nucleatum*. This bacterial strain, acting synergistically with *Streptococcus mutans*, *Aggregatibacter actinomycetemcomitans,* and *Porphyromonas gingivalis* may be the major cause of periodontal and endodontic diseases [51].

Moreover, the *F. nucleatum's* rod shape provides structural support for the adhesion of other bacteria, which will increase the thickness of the polymicrobial biofilm. The reduction in *F. nucleatum* population noticed in Ga-doped samples drastically decreased the biofilm

distribution, and this is particularly evident via SEM analysis (**Fig. 8D)**. In the no-doped zirconia sample, the biofilm covered most of the surface, while in the gallium-coated disc, the biofilm distribution was more limited. In sight of what discussed above, the reason appears clear: the reduction in *F. nucleatum* population impairs biofilm formation or makes the biofilm easy to disrupt [52,53].

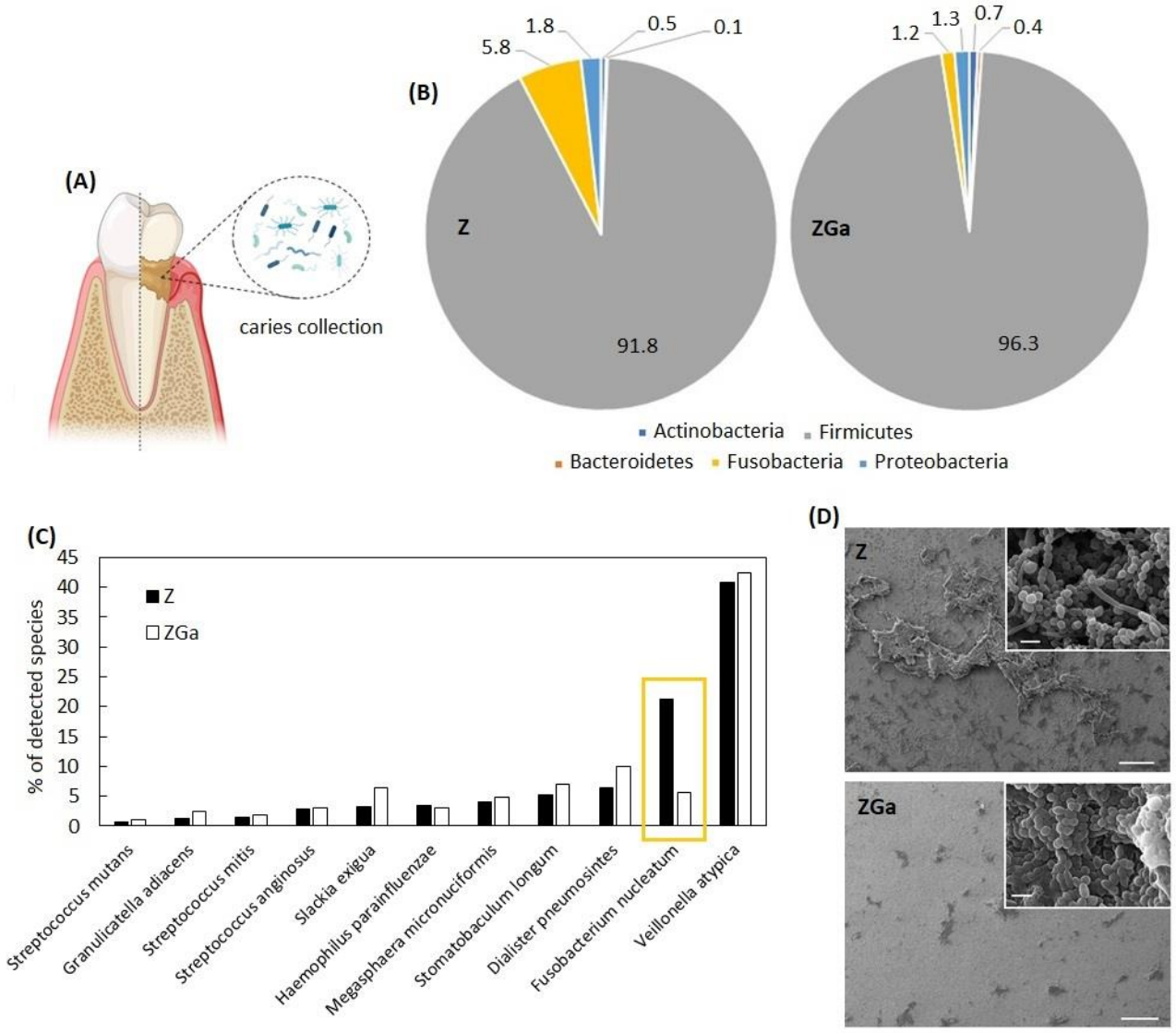

Fig. 8. Pathogens targeted activity. In **(A)** it is represented the oral plaque collection site. **(B)** and **(C)** represents the phylum and the species respectively. The analysis of **(B)** evidence a decrease in the fusobacteria whilst the analysis of **(C)** clearly point out a reduction in *Fusobacterium nucleatum* (in the yellow box); **(D)** show the biofilm distribution on both materials (scale bar 200 µm). The zoomed box (14 Kx, scale bar 1 µm) shows the differences in terms bacterial species. The no doped zirconia coating (Z sample) is rich in fusiform rods bacteria, typical form of *F.*

nucleatum, absent in gallium doped zirconia. This absence may have an impact on biofilm structure stability.

4. Conclusions

In this study tetragonal zirconia coatings were successfully obtained onto bulk zirconia discs through sol-gel spin coating method. Based on *in vitro* studies, the inclusion of gallium ensured promising anti-plaque properties, preserving the normal human oral microbiota. Although, further investigations are required to confirm the biological properties of the zirconia coatings, especially in terms of achieving stability osseo-integration, as well as avoiding inflammation of soft tissue, the current findings promote the use of the herein sol-gel approach to gain novel class of inorganic functional coatings with tailored features useful for improving zirconia dental implants performance.

5. Acknowledgements

Authors would like to acknowledge project PRIN “Multiple Advanced Materials Manufactured by Additive Technologies – PRIN 2017 - prot. 20179SWLKA” and project FESR 2014–2020 ARS01_01205 ‘CustOmmadeaNTibacterical/bioActive/bioCoated Prostheses’ for the economic support.

6 References

[1] R. Smeets, A. Henningsen, O. Jung, M. Heiland, C. Hammächer, J.M. Stein, Definition, etiology, prevention and treatment of peri-implantitis - a review, Head Face Med. 10 (2014) 1–14. doi:10.1186/1746-160X-10-34.

[2] F. Schwarz, J. Derks, A. Monje, H. Wang, Peri-implantitis, J. Clin. Periodontol. 45 (2018) S246–S266. doi:10.1002/JPER.16-0350.

[3] M. Saini, Y. Singh, P. Arora, V. Arora, K. Jain, Implant biomaterials: A comprehensive review., World J. Clin. Cases. 3 (2015) 52–57. doi:10.12998/wjcc.v3.i1.52.

[4] T. Traini, R. Sorrentino, E. Gherlone, F. Perfetti, P. Bollero, F. Zarone, Fracture strength of zirconia and alumina ceramic crowns supported by implants, J. Oral Implantol. 41 (2015) 352–359.

[5] M. Rahmati, M. Mozafari, Biocompatibility of alumina-based biomaterials–A review, J. Cell. Physiol. 234 (2019) 3321–3335.

[6] T. Hanawa, Titanium-tissue interface reaction and its control with surface treatment, Front. Bioeng. Biotechnol. 7 (2019). doi:10.3389/fbioe.2019.00170.

[7] L. Rimondini, L. Cerroni, A. Carrassi, P. Torriceni, Bacterial colonization of zirconia ceramic surfaces: an in vitro and in vivo study., Int. J. Oral Maxillofac. Implants. 17 (2002).

[8] M. Wang, Y. Bai, H. Yang, H. Zou, H. Xia, Y. Wang, Confocal laser scanning microscope evaluation of early bacterial colonization on zirconium oxide and titanium surfaces: An in vivo study, J. Wuhan Univ. Technol. Sci. Ed. 28 (2013) 396–399.

[9] A. Scarano, M. Piattelli, S. Caputi, G.A. Favero, A. Piattelli, Bacterial adhesion on commercially pure titanium and zirconium oxide disks: an in vivo human study, J. Periodontol. 75 (2004) 292–296.

[10] N.B. Arweiler, L. Netuschil, The oral microbiota, Microbiota Hum. Body Implic. Heal. Dis. (2016) 45–60.

[11] I. Salah, I.P. Parkin, E. Allan, Copper as an antimicrobial agent: Recent advances, RSC Adv. 11 (2021) 18179–18186.

[12] J. Pasquet, Y. Chevalier, J. Pelletier, E. Couval, D. Bouvier, M.-A. Bolzinger, The contribution of zinc ions to the antimicrobial activity of zinc oxide, Colloids Surfaces A Physicochem. Eng. Asp. 457 (2014) 263–274.

[13] V. Kumaravel, K.M. Nair, S. Mathew, J. Bartlett, J.E. Kennedy, H.G. Manning, B.J. Whelan, N.S. Leyland, S.C. Pillai, Antimicrobial TiO2 nanocomposite coatings for surfaces, dental and orthopaedic implants, Chem. Eng. J. 416 (2021) 129071. doi:https://doi.org/10.1016/j.cej.2021.129071.

[14] A. Kędziora, R. Wieczorek, M. Speruda, I. Matolínová, T.M. Goszczyński, I. Litwin, V. Matolín, G. Bugla-Płoskońska, Comparison of antibacterial mode of action of silver ions and silver nanoformulations with different physico-chemical properties: Experimental and

computational studies, Front. Microbiol. 12 (2021) 659614.

[15] T. Zhang, L. Wang, Q. Chen, C. Chen, Cytotoxic potential of silver nanoparticles, Yonsei Med. J. 55 (2014) 283–291.

[16] J. Borovanský, P.A. Riley, Cytotoxicity of zinc in vitro, Chem. Biol. Interact. 69 (1989) 279–291.

[17] C.I.Z. O'Hern, K.Y. Djoko, Copper cytotoxicity: cellular casualties of noncognate coordination chemistry, MBio. 13 (2022) e00434-22.

[18] A. Cochis, B. Azzimonti, R. Chiesa, L. Rimondini, M. Gasik, Metallurgical Gallium Additions to Titanium Alloys Demonstrate a Strong Time-Increasing Antibacterial Activity without any Cellular Toxicity, ACS Biomater. Sci. Eng. 5 (2019) 2815–2820.

[19] H. Chouirfa, H. Bouloussa, V. Migonney, C. Falentin-Daudré, Review of titanium surface modification techniques and coatings for antibacterial applications, Acta Biomater. 83 (2019) 37–54. doi:10.1016/j.actbio.2018.10.036.

[20] F.H. Schünemann, M.E. Galárraga-Vinueza, R. Magini, M. Fredel, F. Silva, J.C.M. Souza, Y. Zhang, B. Henriques, Zirconia surface modifications for implant dentistry, Mater. Sci. Eng. C. 98 (2019) 1294–1305.

[21] R. Smeets, B. Stadlinger, F. Schwarz, B. Beck-Broichsitter, O. Jung, C. Precht, F. Kloss, A. Gröbe, M. Heiland, T. Ebker, Impact of Dental Implant Surface Modifications on Osseointegration, Biomed Res. Int. 2016 (2016) 6285620. doi:10.1155/2016/6285620.

[22] M. Djošić, A. Janković, V. Mišković-Stanković, Electrophoretic deposition of biocompatible and bioactive hydroxyapatite-based coatings on titanium, Materials (Basel). 14 (2021). doi:10.3390/ma14185391.

[23] A. D'Agostino, M. Bertolini, N. Bono, M. Pavarini, P. Tarsini, G. Candiani, L. De Nardo, R. Chiesa, Antibacterial titanium dioxide coatings for CoCrMo orthopaedic implants, Appl. Surf. Sci. (2022) 155300.

[24] A.E. Danks, S.R. Hall, Z. Schnepp, The evolution of "sol–gel"chemistry as a technique for materials synthesis, Mater. Horizons. 3 (2016) 91–112.

[25] E. Tranquillo, F. Bollino, Surface Modifications for Implants Lifetime Extension: An Overview of Sol-Gel Coatings, Coatings. 10 (2020) 589. doi:10.3390/coatings10060589.

[26] J. Kim, I.-G. Kang, K.-H. Cheon, S. Lee, S. Park, H.-E. Kim, C.-M. Han, Stable sol–gel hydroxyapatite coating on zirconia dental implant for improved osseointegration, J. Mater. Sci. Mater. Med. 32 (2021) 1–10.

[27] M. Hussain, S.H. Askari Rizvi, N. Abbas, U. Sajjad, M.R. Shad, M.A. Badshah, A.I. Malik, Recent developments in coatings for orthopedic metallic implants, Coatings. 11 (2021) 791.

[28] H. Chouirfa, H. Bouloussa, V. Migonney, C. Falentin-Daudré, Review of titanium surface modification techniques and coatings for antibacterial applications, Acta Biomater. 83 (2019) 37–54.

[29] A. Jaafar, C. Hecker, P. Árki, Y. Joseph, Sol-gel derived hydroxyapatite coatings for titanium implants: A review, Bioengineering. 7 (2020) 1–23. doi:10.3390/bioengineering7040127.

[30] R.B. Figueira, Hybrid sol–gel coatings for corrosion mitigation: a critical review, Polymers (Basel). 12 (2020) 689.

[31] J. Gąsiorek, A. Szczurek, B. Babiarczuk, J. Kaleta, W. Jones, J. Krzak, Functionalizable sol-gel silica coatings for corrosion mitigation, Materials (Basel). 11 (2018) 197.

[32] F. Tana, E. De Giglio, S. Cometa, A. D'Agostino, A. Serafini, F. Variola, N. Bono, R. Chiesa, L. De Nardo, Ca-doped zirconia mesoporous coatings for biomedical applications: A physicochemical and biological investigation, J. Eur. Ceram. Soc. 40 (2020) 3698–3706. doi:https://doi.org/10.1016/j.jeurceramsoc.2019.10.024.

[33] A. D'Agostino, F. Tana, A. Ettorre, M. Pavarini, A. Serafini, A. Cochis, A.C. Scalia, L. Rimondini, E. de Giglio, S. Cometa, R. Chiesa, L. de Nardo, Mesoporous zirconia surfaces with anti-biofilm properties for dental implants, Biomed. Mater. 16 (2021). doi:10.1088/1748-605X/abf88d.

[34] A. Apratim, P. Eachempati, K.K.K. Salian, V. Singh, S. Chhabra, S. Shah, Zirconia in dental implantology: A review, J. Int. Soc. Prev. Community Dent. 5 (2015) 147.

[35] R.B. Osman, M. V Swain, A critical review of dental implant materials with an emphasis on titanium versus zirconia, Materials (Basel). 8 (2015) 932–958.

[36] K. Shahramian, M. Gasik, I. Kangasniemi, X.F. Walboomers, J. Willberg, A. Abdulmajeed, T. Närhi, Zirconia implants with improved attachment to the gingival tissue, J. Periodontol. 91 (2020) 1213–1224.

[37] A. Moreira, S. Madeira, M. Buciumeanu, J. Fialho, A. Carvalho, F. Silva, F.J. Monteiro, J. Caramês, Design and surface characterization of micropatterned silica coatings for zirconia dental implants, J. Mech. Behav. Biomed. Mater. 126 (2022) 105060.

[38] A. C1624-05 (2015), Standard Test Method for Adhesion Strength and Mechanical Failure Modes of, ASTM Int. C1624-5 (2012) 1–29. doi:10.1520/C1624-22.Copyright.

[39] A. Rezvan, E. Sharifikolouei, A. Lassnig, V. Soprunyuk, C. Gammer, F. Spieckermann, W. Schranz, Z. Najmi, A. Cochis, A.C. Scalia, Antibacterial activity, cytocompatibility, and thermomechanical stability of Ti40Zr10Cu36Pd14 bulk metallic glass, Mater. Today Bio. 16 (2022) 100378.

[40] J. Brandi, S. Cheri, M. Manfredi, C. Di Carlo, V. Vita Vanella, F. Federici, E. Bombiero, A. Bazaj, E. Rizzi, L. Manna, Exploring the wound healing, anti-inflammatory, anti-pathogenic and proteomic effects of lactic acid bacteria on keratinocytes, Sci. Rep. 10 (2020) 11572.

[41] R. Gurdeep Singh, A. Tanca, A. Palomba, F. Van der Jeugt, P. Verschaffelt, S. Uzzau, L. Martens, P. Dawyndt, B. Mesuere, Unipept 4.0: functional analysis of metaproteome data, J. Proteome Res. 18 (2018) 606–615.

[42] R.C. Garvie, Stabilization of the tetragonal structure in zirconia microcrystals, J. Phys.

Chem. 82 (1978) 218–224.

[43] J. Moussi, J.L. Drury, J.C. Wataha, Zirconia in biomedical applications AU - Chen, Yen-Wei, Expert Rev. Med. Devices. 13 (2016) 945–963. doi:10.1080/17434440.2016.1230017.

[44] P. AmyáTsai, Formation and prevention of fractures in sol–gel-derived thin films, Soft Matter. 11 (2015) 882–888.

[45] W. Zai, C.L. Wu, H.C. Man, Improving adhesion strength of sol-gel coating on CoCrMo by electrochemical pretreatment, Mater. Lett. 270 (2020) 127696.

[46] F. Rupp, R.A. Gittens, L. Scheideler, A. Marmur, B.D. Boyan, Z. Schwartz, J. Geis-Gerstorfer, A review on the wettability of dental implant surfaces I: theoretical and experimental aspects, Acta Biomater. 10 (2014) 2894–2906.

[47] S. Kligman, Z. Ren, C.-H. Chung, M.A. Perillo, Y.-C. Chang, H. Koo, Z. Zheng, C. Li, The impact of dental implant surface modifications on osseointegration and biofilm formation, J. Clin. Med. 10 (2021) 1641.

[48] D.G. Tamay, S. Gokyer, J. Schmidt, A. Vladescu, P. Yilgor Huri, V. Hasirci, N. Hasirci, Corrosion Resistance and Cytocompatibility of Magnesium–Calcium Alloys Modified with Zinc-or Gallium-Doped Calcium Phosphate Coatings, ACS Appl. Mater. Interfaces. 14 (2021) 104–122.

[49] C.H. Goss, Y. Kaneko, L. Khuu, G.D. Anderson, S. Ravishankar, M.L. Aitken, N. Lechtzin, G. Zhou, D.M. Czyz, K. McLean, O. Olakanmi, H.A. Shuman, M. Teresi, E. Wilhelm, E. Caldwell, S.J. Salipante, D.B. Hornick, R.J. Siehnel, L. Becker, B.E. Britigan, P.K. Singh, Gallium disrupts bacterial iron metabolism and has therapeutic effects in mice and humans with lung infections, Sci. Transl. Med. 10 (2018) eaat7520. doi:10.1126/scitranslmed.aat7520.

[50] C.A. Brennan, W.S. Garrett, Fusobacterium nucleatum—symbiont, opportunist and oncobacterium, Nat. Rev. Microbiol. 17 (2019) 156–166.

[51] J. Zhu, W. Chu, J. Luo, J. Yang, L. He, J. Li, Dental materials for oral microbiota dysbiosis: An update, Front. Cell. Infect. Microbiol. (2022) 907.

[52] D.J. Bradshaw, P.D. Marsh, G.K. Watson, C. Allison, Role of Fusobacterium nucleatum and coaggregation in anaerobe survival in planktonic and biofilm oral microbial communities during aeration, Infect. Immun. 66 (1998) 4729–4732.

[53] S. Groeger, Y. Zhou, S. Ruf, J. Meyle, Pathogenic Mechanisms of Fusobacterium nucleatum on Oral Epithelial Cells, Front. Oral Heal. 3 (2022).